Chapter 13
Trends in High-Speed Interconnects for Datacenter Networking: Multidimensional Formats and Their Enabling DSP

David V. Plant, Mohamed H. Morsy-Osman, Mathieu Chagnon, and Stephane Lessard

13.1 Introduction

The role of Internet in every facet of nowadays society is indisputable. Growing Internet traffic due to fast-expanding bandwidth intensive applications across all sectors (e.g., social networking, cloud computing and storage, e-commerce, etc.) is creating a spurring capacity demand in DCs. Driven by the persistent growth of cloud-based business and consumer services, the datacenter (DC) traffic is growing incessantly. Its global estimate is forecasted to reach more than 15 zettabytes (1 zetta = 10^{21}) by 2020 representing more than threefold increase from its 2015 value [1]. Nowadays, the majority of Internet traffic, which used to be dominated by peer-to-peer traffic, originates or terminates at a DC. Approximately 77% of traffic originating from a DC is predicted to stay within the DC in 2020 [1]. Also, *hyper-scale data centers*, which already account for 34% of total DC traffic, will account for 53% by 2020 [1]. This relentless growth of intra-DC traffic and DC sizes is driving the need for fast inexpensive short-reach optics that provides the desired capacity over growing intra-DC reaches (<10 km). Inside these mega warehouse-sized DCs (see Fig. 13.1), several hundreds of thousands of servers that store and process massive amounts of cloud data reside in large racks (see Fig. 13.2). Typically, servers within each rack are interconnected using a *top-of-rack (ToR) switch*, and several ToRs are connected through *aggregate switches* [2]. According to [3], current generation top-of-rack (ToR) switches have a switching capacity of 3.2 Tbps that is

D.V. Plant (✉) • M.H. Morsy-Osman • M. Chagnon
Department of Electrical & Computer Engineering, McGill University, Montréal, QC H3A 2A7, Canada
e-mail: david.plant@mcgill.ca; mohamed.osman2@mcgill.ca; mathieu.chagnon@mail.mcgill.ca

S. Lessard
Ericsson Research, 8275 Route Transcanadienne, Saint-Laurent, QC H4S 0B6, Canada
e-mail: stephane.lessard@ericsson.com

F. Testa, L. Pavesi (eds.), *Optical Switching in Next Generation Data Centers*,
DOI 10.1007/978-3-319-61052-8_13

Fig. 13.1 Google's large DC facility in Council Bluffs, Iowa

Fig. 13.2 Racks containing hundreds of thousands of servers inside a Google DC

usually provided across 32 ports, each port hosting an optical transceiver that is typically a *Quad Small Form-Factor Pluggable 28* (QSFP28) attached to the switch faceplate. Each QSFP28 provides a net throughput of 100 Gb/s using 4 × 25 Gb/s lanes. Next-generation ToR switch capacities are expected to be 6.4 and 12.8 Tb/s. In order for switches to provide the desired throughput while maintaining a reasonable port density in 1 rack unit (RU) form factor, the number of lanes per transceiver needs to increase by utilizing more wavelengths or fiber lanes in a *wavelength division multiplexing* (WDM) or *space division multiplexing* (SDM) scheme,

respectively. However, this is not a scalable solution due to packaging difficulties that exacerbate upgrade to higher capacities using multiplexing approaches. A more promising approach is to employ advanced modulation formats to increase the bit rate per wavelength (per carrier) and hence reduce the required wavelengths or fiber lanes to achieve the target aggregate throughput. Modulating multiple dimensions of a lightwave over numerous levels allows increasing binary throughputs of single-channel short-reach transceivers while maintaining a cost-effective *self-beating* DD scheme. The abovementioned trend can be also observed by the adoption of *pulse amplitude modulation* over four levels (PAM4) as the modulation format to use in the upcoming 400G Ethernet standard over intra-DC reach replacing legacy on-off keying (OOK) that operated over two levels in past standards [4]. Compared to *coherent detection*, direct detection (1) employs a simpler front-end that does not have a local oscillator (LO), (2) requires simpler DSP since there is no need for laser phase noise and frequency offset compensation, and (3) can operate without thermoelectric coolers (TECs), all of which resulting in a receiver that is inexpensive, compact, and less power hungry.

In this chapter, we present a review of the recent literature of multidimensional modulation and direct detection systems that deliver large bit rates (>100 Gb/s) per wavelength over *short reach* for intra-DC interconnects. We begin by reviewing the mathematical representation of a lightwave and polarization rotation in Stokes space. Then, we present the evolution of the multidimensional modulation formats depicting the architectures of their respective transmitters and receivers. Next, digital signal processing (DSP) functions that enable using direct-detection receivers for such formats are presented. Then, the key results that have been recently reported are summarized. Finally, we conclude and give potential future research directions.

13.2 Representation of a Lightwave and Polarization Rotation in Jones and Stokes Spaces

In this section we introduce different notations to represent an optical field in *single mode fiber* (SMF). SMF are cylindrical waveguides that can support the propagation of two orthogonal complex fields. There are two principal ways to vectorially represent the whole optical field in SMF: the Jones and Stokes representations [5]. Both are based on a reference polarization coordinate system. The *Jones space* is a two-dimensional complex space where each dimension represents an orthogonal state of polarization (SOP) of the light and where the argument of each dimension is the complex optical field in said dimension, providing in total 4 degrees of freedom (DOF). These complex two-dimensional Jones vectors are more concisely expressed using "bra-ket notation," where the "ket" is written as $|E\rangle = [E_x, E_y]^T$ and the "bra" is $\langle E| = |E\rangle^\dagger = \left[E_x^*, E_y^*\right]$, where * represents complex conjugation, † the conjugate transpose, and ^{T} the transpose. The fields E_x and E_y are the complex fields on the $\hat{x}$

and $\hat{y}$ polarizations, respectively. The same field can be equivalently represented in Stokes space using a three-dimensional (3D) real-valued vector $\boldsymbol{S} = [S_1, S_2, S_3]^{\mathrm{T}}$, where $S_1 = E_x^* E_x - E_y^* E_y$, $S_2 = 2\,\mathrm{Re}\{E_x E_y^*\}$, and $S_3 = -2Im\{E_x E_y^*\}$. By definition, Stokes vectors bear the property that $\left(S_1^2 + S_2^2 + S_3^2\right)^{1/2} = E_x^* E_x + E_y^* E_y$, being the total power. Stokes vectors have only 3 degrees of freedom, being the power on $\hat{x}$, the power on y, and phase difference between the two polarizations E_x and E_y. In order to have a direct access to the total power in the vector representation, the latter can be added to the Stokes vector $\boldsymbol{S}$ as $\boldsymbol{S}' = [S_0, S_1, S_2, S_3]^{\mathrm{T}}$, where S_0 is the total power. The vector $\boldsymbol{S}'$ is called the *Mueller vector* [6]. For direct access to the first two degrees of freedom, it is also common to cast the four-component Mueller vector in the form $\boldsymbol{V} = [E_x^* E_x, E_y^* E_y, S_2, S_3]^{\mathrm{T}}$, where the first two components of $\boldsymbol{S}'$ and $\boldsymbol{V}$ are related as $E_x^* E_x = \left(S_0 + S_1\right)/2$ and $E_y^* E_y = \left(S_0 - S_1\right)/2$. From the representation of the first two components, we will call this modified Mueller vector $\boldsymbol{V}$ the *power vector*. We will use this vector representation in the remaining sections of this manuscript as the reference field representation. It is noteworthy to mention that the presence of complex conjugation in all four Stokes components S_0 to S_3 cancels any absolute phase information in Stokes space, hence the loss of a DOF from four in Jones to three in all variants of Stokes representations.

In single-mode fibers being non-polarization-maintaining fibers, the field inside the latter undergoes polarization rotations due to inherent random *birefringence* [5]. The following Eqs. (13.1–13.2) present the impact of polarization rotation in SMF on both Jones and modified Mueller representations. In complex Jones space, a rotation is a complex unitary matrix **U** applied to the Jones vector $|E\rangle$ as

$$\left|E_{\mathrm{rot}}\right\rangle = \mathbf{U}\left|E\right\rangle = \begin{bmatrix} a & -b \\ b^* & a^* \end{bmatrix} \left|E\right\rangle \tag{13.1}$$

where unitary matrices have the property that $\mathbf{U}^{\dagger}\mathbf{U} = \mathbf{I}$, the identity matrix. In the power vector representation, the equivalent rotation on $\boldsymbol{V}$ is cast as $\boldsymbol{V}_{\mathbf{rot}} = \mathbf{M}\boldsymbol{V}$ [6] where the rotation matrix **M** is given by

$$\mathbf{M} = \begin{bmatrix} |a|^2 & |b|^2 & -\mathrm{Re}\{ab^*\} & -Im\{ab^*\} \\ |b|^2 & |a|^2 & \mathrm{Re}\{ab^*\} & -Im\{ab^*\} \\ 2\,\mathrm{Re}\{ab\} & -2\,\mathrm{Re}\{ab\} & \mathrm{Re}\{a^2\} - \mathrm{Re}\{b^2\} & Im\{a^2\} + Im\{b^2\} \\ 2Im\{ab\} & -2Im\{ab\} & Im\{b^2\} - Im\{a^2\} & \mathrm{Re}\{a^2\} + \mathrm{Re}\{b^2\} \end{bmatrix} \tag{13.2}$$

Because power vectors *V* are always real valued, 4-by-4 rotation matrix M is also real valued.

13.3 Evolution of Multidimensional Modulation Formats and Their Transceiver Architectures

Figure 13.3 summarizes the evolution of the dimensionality (N_{dim}) of modulation formats and their underlying transmitter and receiver architectures for self-beating direct detect optical communication systems for 1D, 2D, 3D, and 4D modulation, i.e., for $N_{\text{dim}} = \{1, 2, 3, 4\}$. The figure is complemented with example formats and their corresponding field representation in the optical domain.

Increasing the bit rate of single carriers employing 1D modulation formats ($N_{\text{dim}} = 1$) requires either (1) increasing the symbol rate or (2) increasing the modulation complexity imprinted on this dimension. Faster signaling requires electronics of larger bandwidth, while increased modulation complexity improves the spectral efficiency at the expense of requiring a more complex electrical drive signal. The laser drive signal, and therefore the signal obtained after direct detection, can be simple binary signals or more complex waveforms. The most flexible way to generate complex waveforms is to employ a digital-to-analog converter (DAC) of large bit resolution. Several different modulation formats have recently been demonstrated to increase the spectral efficiency, such as discrete multitone modulation (DMT) [7], half-cycle 16-QAM Nyquist-subcarrier-modulation [8], multiband carrier-less amplitude phase modulation (CAP) [9], and multilevel intensity modulation, also known as pulse amplitude modulation (PAM) [10]. All these formats are greatly leveraged by digital signal processing (DSP) from a DAC, while some (e.g., DMT) inherently require a DAC and DSP. Electrical multilevel signaling, on the other hand, can be generated in a simpler way without a DAC by power combining NRZ two-level tributaries of different amplitudes.

Intensity modulation of a laser can be done using direct modulated lasers (DML), electroabsorption-integrated modulated lasers (EML), or via a Mach-Zehnder modulator (MZM) [11]. The receiver for 1D formats is a simple photodiode, converting the total optical power $\langle E|E\rangle$ into photocurrent. For some 1D IM formats employing higher-order modulation like DMT, the receiver also has to comprise an ADC and a DSP block [7], while any format can benefit from digital signal equalization. The "1D" line of Fig. 13.3 depicts the transmitter and receiver architectures for 1D formats, where dashed boxes represent a DAC- or ADC-based transceiver with DSP.

The current technology for optical Ethernet pluggables in datacenters relies on 1D OOK intensity modulation on a single polarization (SP-OOK). Such format provides 1 bit per symbol. To increase the binary throughput of these pluggables, multiple carriers are independently modulated and multiplexed on either different wavelengths in a fiber or on different fibers representing either wavelength division multiplexing (WDM) or space division multiplexing (SDM), respectively. The transceiver requires as many parallel transmitters (RF signals, amplifiers, electro-optic transducers) and parallel receivers (optoelectronic transducers, amplifiers, detectors) as the multiplexing order. Though these multiplexing solutions are currently adopted, they are not scalable toward future larger aggregate bit rates.

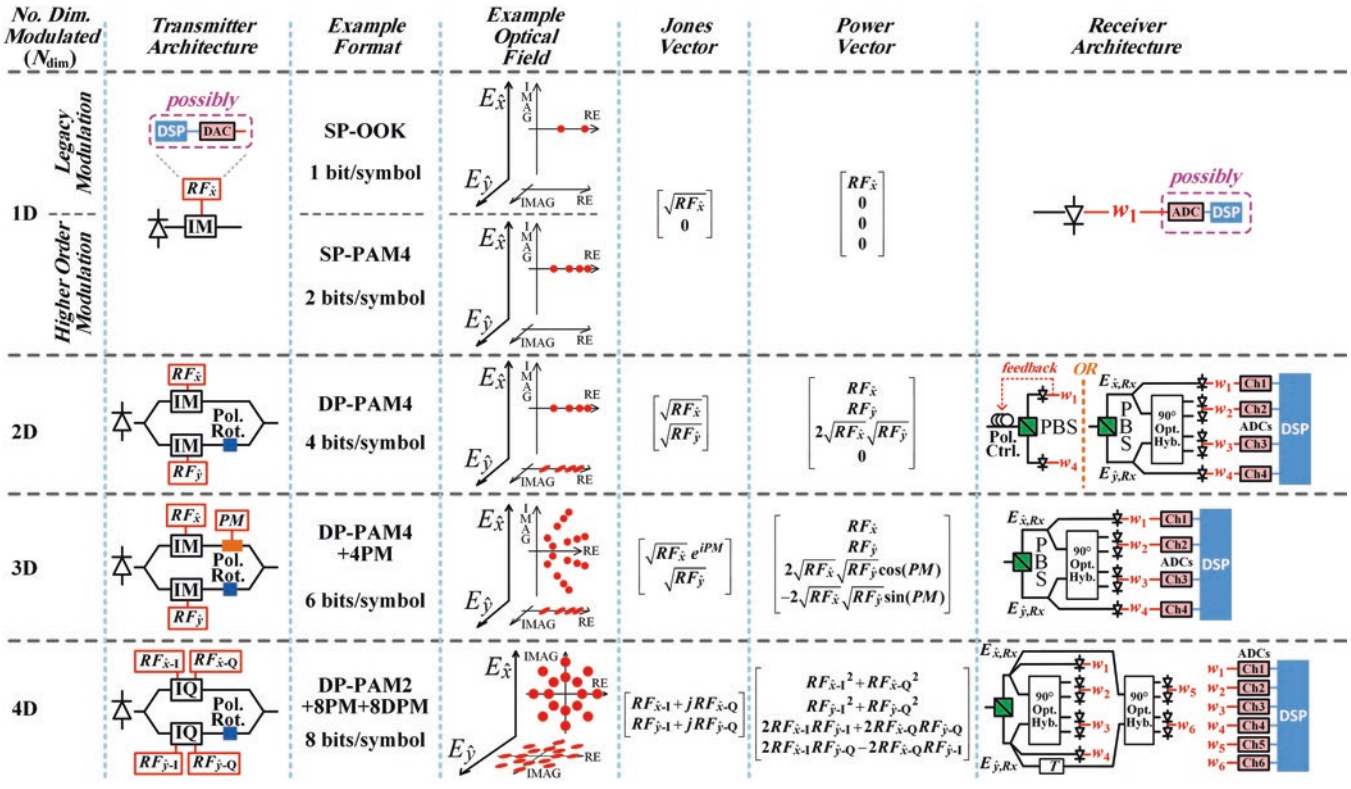

Fig. 13.3 Evolution of transceiver architectures for 1D, 2D, 3D, and 4D formats for self-beating direct detection systems

Although increasing the modulation order of electrical 1D formats improves the bit rate delivered by improving the spectral efficiency, it comes with an increase of the BER because the SNR remains unchanged [10]. Higher order intensity modulation provides a good example to express this phenomenon. The BER of multilevel formats is function of the SNR and the number of levels M as expressed in Eq. (13.3):

$$\underset{\text{PAM M}}{\text{BER}}\left(M,\text{SNR}\right)=\frac{M-1}{M\log_2\left(M\right)}erfc\left(\sqrt{\frac{3}{2\left(M^2-1\right)}\text{SNR}}\right) \tag{13.3}$$

where *erfc* is the complementary error function.

If a two-level intensity modulated signal providing 1 bit/symbol has a SNR of 16.94 dB, increasing the number of levels to four or eight to double or triple the bit rate worsens the BER from 1×10^{-12} to 6.2×10^{-4} or 3.6×10^{-2}, respectively. Conversely, to maintain the BER at four- and eight-level intensity signaling, the SNR has to increase to 23.88 and 30.07 dB, respectively. In the "1D" line of Fig. 13.3, we depict the symbols in the optical field of both two- and four-level 1D intensity modulation, where both formats have the same mean "DC" and "AC" signal power. By visual inspection, one can observe that the symbol spacings are much closer at four levels, explaining the increase of the BER. Symbols in the optical field are spaced in a square-root fashion such to generate equally spaced levels after square-law direct detection.

Binary throughputs from a single carrier direct detect systems can be further increased by modulating more dimensions of a lightwave, i.e., $N_{\text{dim}} > 1$. In the following, with visual inspections from Fig. 13.3, we present transceiver architectures and corresponding optical fields of 2D, 3D, and 4D format compliant to self-beating direct detection.

One variant of 2D formats is to modulate independently the intensity on each orthogonal polarization. Such format is called *dual-polarization intensity modulation* (DP-IM) and allows to double the bitrate of 1D IM format while maintaining the signaling rate and without affecting the SNR per orthogonal polarization [12]. The transmitter architecture for such 2D format requires two driving signals and intensity modulators, branched off of the same laser source and combined on orthogonal polarizations, thanks to an inline polarization rotator (Pol. Rot.), as depicted in the "2D" line of Fig. 13.3. Other variants of 2D transmitters employ complex IQ modulation on one polarization while sending a copy of the CW transmit laser on the orthogonal polarization [13–15]. For these 2D formats, two different types of receiver can recover the two intensities which are differentiated by the method employed to cancel polarization rotation: optically or digitally.

The first receiver performs polarization derotation in the optical domain and consists of an active polarization controller followed by a polarization beam splitter (PBS) serving as a polarization demultiplexer, where the two outputs are subsequently detected by a photodiode. The two resulting RF photocurrents can be input

to ADCs for subsequent DSP for IM formats having complex modulation schemes, like DMT, or where digital filtering is applied to enhance BER performance, like in the case of 1D formats. Other simpler IM formats relying on multilevel modulation can be detected without DSP, although digital filtering tends to improve the BER performance. As polarization slowly wanders inside single-mode fiber (see Eqs. (13.1) and (13.2)), it needs to be tracked such to maintain the two optical outputs of the PBS using a control signal from one of the two photocurrents. The control signal minimizes the inter-polarization crosstalk on said RF output. Such receiver architecture is depicted at the end of the "2D" line of Fig. 13.3.

The other type of receiver for 2D formats is called a *Stokes vector receiver* (SVR) and uses digital signal processing to perform *polarization derotation* [12]. The receiver architecture, also depicted at the end of the "2D" line of Fig. 13.3, is comprised of a PBS where each output is further split in two using couplers. The couplers' outputs from orthogonal polarizations are combined together on the same polarization through a 90° optical hybrid, and the four hybrid outputs are detected in pairs using balanced photodetectors. The other couplers' outputs of each polarization are directed to photodetectors. The four photocurrents generated are real time sampled using four analog-to-digital converters (ADC) and are input to subsequent DSP. The four waveforms w_1 to w_4 are $\left|E_{x,Rx}\right|^2$, $2\,\mathrm{Re}\left\{E_{x,Rx}\,E_{y,Rx}^{*}\right\}$, $2Im\left\{E_{x,Rx}\,E_{y,Rx}^{*}\right\}$, and $\left|E_{\hat{y},Rx}\right|^2$, respectively, and represent the four components of the rotated modified Mueller power vector introduced in Sect. 2. The DSP algorithm employed to recover the two intensity tributaries is that for 2D formats presented in Sect. 4 and performs polarization derotation and allows for mitigation of *intersymbol interference* (ISI). It is noteworthy to mention that the active optical polarization tracking of the first 2D receiver is now replaced by active digital polarization tracking and the optical receiver front-end of SVR is a passive structure serving to beat the incoming signal with itself.

The "3D" line of Fig. 13.3 presents the transmitter architecture allowing to modulate a third orthogonal degree of freedom while maintaining a direct detection scheme, therefore permitting to triple the bit rate of 1D formats, while the signaling rate stays the same [16]. The transmitter architecture is similar to that of 2D formats, with an additional phase modulator in one of the two IM branches. This phase modulator allows modulating the *inter-polarization phase*: the phase of one polarization with respect to the other orthogonal polarization. When all three driving signals are of four-level modulation, the optical signal carries 6 bits per symbol. The optical field of such format, called dual polarization PAM4 with four inter-polarization phases (DP-PAM4 + 4 PM), is also depicted in Fig. 13.3. The same SVR receiver for 2D formats can be used to recover all three degrees of freedom via the received modified Mueller power vector using the DSP presented in Sect. 4 for "3D" formats, where now all four components of V_{4D} need to be derotated and recovered digitally.

Finally, it is possible to modulate a fourth dimension of the optical field and recover the latter in a direct detect fashion [17]. Similar to differential phase shift keying (DPSK) modulation, the phase jumps from one Jones vector symbol to the next can be modulated and demodulated using self-beating. Unlike DPSK, there are three possible intersymbol phase jumps that can be modulated: phase jumps from $E_x[\mathrm{n}]$ to $E_x[\mathrm{n}+1]$, from $E_y[\mathrm{n}]$ to $E_y[\mathrm{n}+1]$, or from $E_x[\mathrm{n}]$ to $E_y[\mathrm{n}+1]$, where n is the discrete time index at time $t = \mathrm{n}T$ and where T is the symbol duration. The transmitter architecture to generate the format differs from that of the previous 2D and 3D formats. Instead of employing intensity and phase modulators, the transmitter uses in-phase-quad-phase (IQ) modulators, also known as dual-parallel Mach-Zehnder modulator (MZM), where each MZM is biased at null. The transmitter comprises two IQs modulating independently, in a complex fashion, the same laser source where the polarization of one IQ output is rotated such to combine the two tributaries on orthogonal polarizations. This transmitter architecture is the same as that for polarization-multiplexed coherent transmission, serving as a full four-dimensional field modulator, as depicted in "4D" line of Fig. 13.3. Only specific complex modulation formats relying on multi-ring/multiphase can be employed in order to be recoverable by a self-beating receiver [17]. To demodulate the intersymbol, inter-polarization phase jumps in a self-beating fashion, the SVR used for 2D and 3D formats has to be modified as depicted in the receiver architecture column of the "4D" line of Fig. 13.3, where the received field $E_{x,Rx}$ beats with a one symbol delayed version of $E_{y,Rx}$ through a second 90° optical hybrid. Waveforms w_1 to w_4 are the same as that of the SVR for 2D and 3D formats, and w_5 and w_6 are $2\,\mathrm{Re}\left\{E_{x,Rx}[n]E_{y,Rx}[n-1]\right\}$ and $-2Im\left\{E_{x,Rx}[n]E_{y,Rx}[n-1]\right\}$, respectively.

13.4 Enabling DSP for Multidimensional Formats

All modulation formats outlined in the previous section benefit from applying DSP at the transmitter and receiver sides; some of these DSP tasks are mandatory since they, for example, enable polarization demultiplexing in a multidimensional format ($N_{\mathrm{dim}} > 1$) or compensate for a significant amount of ISI due to limited bandwidth of electronics. Figure 13.4a shows a high-level block diagram of the DSP stack of possible functions carried out at the transmitter for a N_{dim}-D format. We assume each dimension of the lightwave carries one symbol that is drawn from a symbol alphabet with size K. This leads to having $N_{\mathrm{dim}}\log_2 K$ bits that get modulated per symbol across all dimensions of the lightwave. Subsequent DSP blocks at the transmitter include: (1) resampling to the sampling rate of the digital-to-analog converter (DAC) if used, (2) pulse shaping using a band-limiting spectral shaping filter, (3) compensation of the nonlinear (NL) transfer characteristics of a Mach-Zehnder modulator (MZM) if used, (4) pre-compensation of ISI using a finite impulse

response (FIR) filter, and (5) clipping and quantizing the resulting samples in preparation of feeding them to a DAC having a finite number of bits to represent each quantized level. The chain of the abovementioned DSP functions is applied to all N_{dim} signals that will modulate each of the N_{dim} dimensions of the lightwave. However, some the above functions may not be used for all dimensions. For example, the driving signal that gets imprinted onto the inter-polarization phase does not require any compensation of the NL characteristics of a MZM since it drives a linear phase modulator (PM), not a MZM (refer to the 3D transmitter architecture in Fig. 13.3). Next, Fig. 13.4b shows a high-level block diagram of the DSP stack of possible functions carried out at the receiver for a N_{dim}-D format. Depending on N_{dim}, we assume the input signal to the receiver DSP chain comprises N_{ch} waveforms provided by the ADCs that sample each of the output photocurrents from one the corresponding receiver front-ends in Fig. 13.3. After resampling from the sampling rate of the ADC to twice the symbol rate, the key DSP block at the receiver is a *multiple-input*, *multiple-output* (MIMO) bank of FIR filters each having a temporal length N_{taps}. The task of the bank of FIR filters is twofold: (1) it achieves polarization demultiplexing by inverting the polarization rotation that occurs along the fiber (refer to Eqs. 13.1 and 13.2 in Sect. 2) which results in a misalignment between the transmitter's and receiver's principle axes, denoted by $(\hat{x}, \hat{y})_{Tx}$ and $(\hat{x}, \hat{y})_{Rx}$, and (2) it post-compensates any residual ISI that may have resulted from bandwidth-limited electronic components in the system (e.g., electric amplifiers, ADCs, DACs, etc.). The final two blocks in the receiver DSP chain include clock recovery and hard decision of the received symbols on each of the N_{dim} dimensions. Clearly, the key enabling DSP block in the chains of Fig. 13.4 is the MIMO filtering. This block accepts N_{ch} incoming signals from the receiver front-end and provides N_{dim} signals ready for the retiming and final decision. Henceforth, we explain in detail the contents of the MIMO filtering block for each of the multidimensional formats, i.e., for $N_{\text{dim}} = \{2, 3, 4\}$.

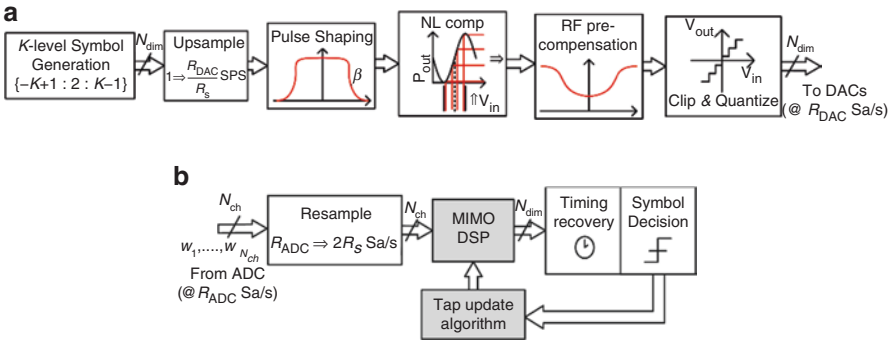

Fig. 13.4 High-level block diagrams of possible DSP functions at (**a**) transmitter and (**b**) receiver, for a N_{dim}-D modulation format. The transmitter DSP stack generates N_{dim} signal streams that drive N_{dim} DAC channels each running at R_{DAC} Sa/s. The receiver DSP chain accepts N_{ch} waveforms from N_{ch} ADC channels each running at R_{ADC} Sa/s from the Stokes receiver front-end depicted earlier in Fig. 13.3

Since 1D formats are detected via a single photodetector which is agnostic to the received state of polarization (SOP), the DSP at the receiver side (if used at all) is useful to post-compensate any residual ISI. Hence the MIMO block in Fig. 13.4b reduces to a single-input, single-output (SISO) FIR filter that post-compensates ISI [18]. On the other hand, 2D, 3D, and 4D formats are severely impacted by the cross-talk resulting from the misalignment of the transmitter's and receiver's principle axes due to random polarization rotation. Hence, MIMO DSP is mandatory to undo the polarization rotation and recover the transmitted data. Figure 13.5a shows a block diagram of the MIMO DSP required for the 2D DP-IM format as was detailed

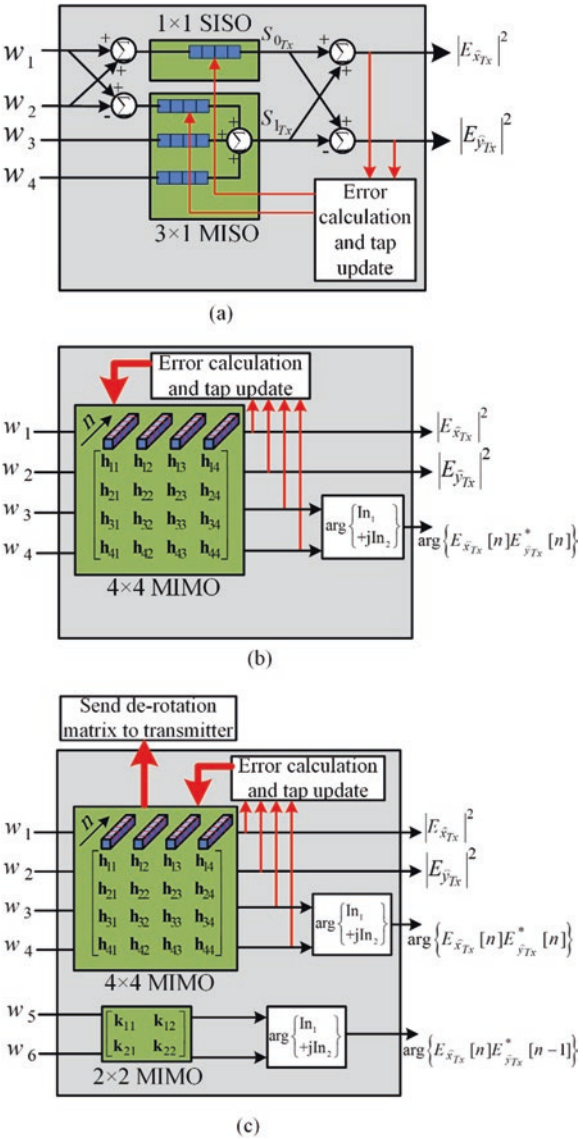

Fig. 13.5 Structural block diagrams of MIMO DSP that follows the Stokes receiver front-end for (**a**) 2D DP-IM, (**b**) 3D DP-IM-PM, and (**c**) 4D DP-IM-PM-DPM modulation formats

in [19]. The block comprises a combination of one SISO FIR filter and a 3 × 1 multiple-input, single-output (MISO) bank of FIR filters that accepts four waveforms w_1 to w_4 from the front-end in the 2D line of Fig. 13.3 giving the transmitted intensities $\left|E_{\hat{x},Tx}\right|^2$ and $\left|E_{\hat{y},Tx}\right|^2$. In such case, the 3 × 1 MISO block (a) provides the inversion of the polarization rotation, and the temporal length of all the filters is to mitigate the ISI. In case of 3D DP-IM-PM format, the MIMO block required becomes the one in Fig. 13.5b which accepts the same four waveforms w_1 to w_4 from the respective front-end in Fig. 13.3 and recovers $\left|E_{\hat{x},Tx}\right|^2$ and $\left|E_{\hat{y},Tx}\right|^2$ as well as the inter-polarization phase $\arg\left\{E_{\hat{x},Tx}\,E^*_{\hat{y},Tx}\right\}$ [6] − arg $\{S_{2\mathrm{Tx}}+\boldsymbol{i}\boldsymbol{S}_{3\mathrm{Tx}}\}$. In such case, the 4 × 4 MIMO is adapted so that it inverts the polarization rotation besides the temporal length of each FIR filter to remove residual ISI. Finally, the 4D DP-IM-PM-DPM format in [17] requires processing the two additional waveforms w_5 and w_6 from the front-end in the last line of Fig. 13.3. For such 4D format, the MIMO block becomes the one in Fig. 13.5c where the first four waveforms w_1 to w_4 are processed in exactly the same manner as in Fig. 13.5b for the 3D format. As clearly explained in [20], recovering the fourth dimension from w_5 and w_6 is only possible if $\left(\hat{x},\hat{y}\right)_{Tx}$ and $\left(\hat{x},\hat{y}\right)_{Rx}$ are aligned. In order to align the transmitter's and receiver's axes, we make use of the knowledge of the derotation matrix that is obtained from 4 × 4 MIMO operating on the first three dimensions. This matrix is sent back to the transmitter where the DP-IQ modulator can pre-rotate the transmitted waveforms, ensuring aligned axes at the receiver. In such case, w_5 and w_6 can be processed separately by a 2 × 2 MIMO block that recovers the fourth dimension: the inter-polarization differential phase $\arg\left\{E_{\hat{x},Tx}[\mathrm{n}]E^*_{\hat{y},Tx}[\mathrm{n}-1]\right\}$.

13.5 State-of-the-Art Experimental Results Using Transceivers Realized by Discrete Components

This section summarizes the key results achieved using the modulation formats whose details and transceiver architectures were presented in Sect. 3 and are enabled using the DSP presented in Sect. 4. Table 13.1 presents the summary of the key results achieved using 1D, 2D, 3D, and 4D formats; each is listed in a separate row. Specifics of the experimental testbeds used for each experiment can be found in the publications cited in the table. All these record-breaking results were generated at the labs of the Photonics Systems Group (PSG) at McGill University. Figure 13.6 shows photos of the testbed used to demonstrate the 2D DP-PAM4 format that generated the results in [19]. Key modulation parameters for each experiment are listed including the symbol rate (or baud rate), the resulting number of bits per symbol, the maximum transmission distance or reach, and the operating wavelength.

Table 13.1 Summary of key achievements using multidimensional formats relying on direct-detection receivers with polarization demultiplexing using DSP (HD-FEC: Hard decision forward error correction)

Number of dimensioNumber of dimensions	Modulation format	Number of bits per symbol	Baud rate (Gsym/s)	Maximum bit rate (Gb/s) achieved at HD-FEC	Transmission distance (km)	Operating wavelength (nm)
1D [18]	PAM4 or PAM8	2 or 3	56 or 37.4	112	10	1310
2D [19]	DP-PAM4	4	56	224	10	1310
3D [6]	DP-PAM4-4 PM	6	50	300	b2b	1550
4D [20]	DP-PAM2-8 PM-8DPM	8	40	320	10	1550

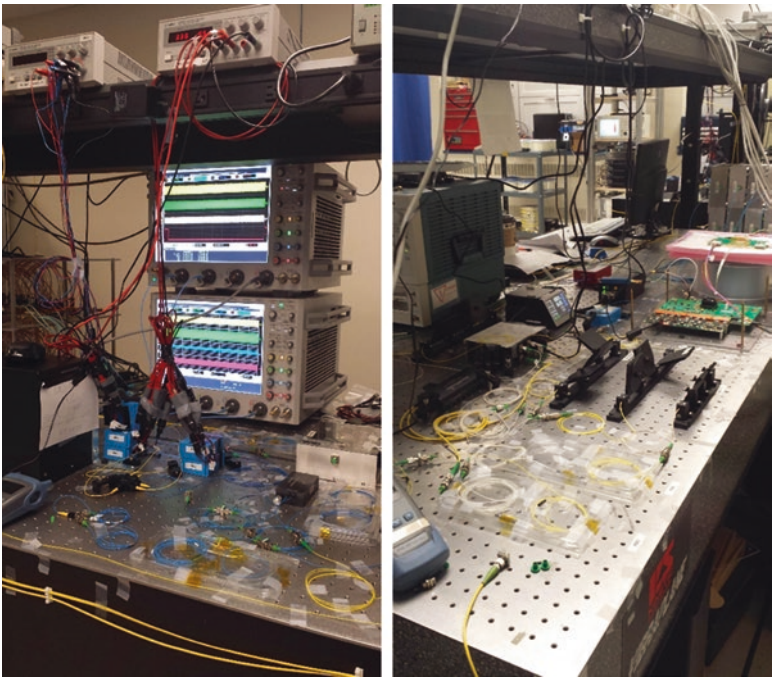

Fig. 13.6 Photos captured at the Photonics Systems Group Lab at McGill University for the experimental setup to demonstrate the 2D DP-PAM4 format in [19]. *Left* photo is the Stokes vector receiver front-end realized using discrete components followed by real-time scopes, and *right* photo is the DP-PAM4 transmitter

Also, Table 13.1 lists the maximum bit rate we were able to achieve using each format, while the bit error rate (BER) stays below the hard decision forward error correction (HD-FEC) threshold of 3.8×10^{-3}. If the BER stays below HD-FEC, the FEC decoder that follows the receiver DSP chain in Fig. 13.4b is guaranteed to produce error-free decoded bits with post-FEC BER in the range of 10^{-12} to 10^{-15} depending on the type of FEC used.

Examining Table 13.1 carefully, we notice that going from one row to the next, the number of modulated dimensions increases meaning more bits per symbol are modulated; hence, the resulting capacity (bit rate) per carrier goes up. Also, we notice that the first two experiments in [18, 19] for 1D and 2D formats were performed in the O band (1310 nm) near the zero dispersion wavelength of standard single-mode fiber (SMF), and hence the only factor that limited the maximum transmission distance is the received power budget. For the following experiment in [6] for the 3D format which was done in the C band (1550 nm) due to availability of parts, the interplay between dispersion and phase modulation limited the transmission distance severely, and we were only able to demonstrate the feasibility of the format in back to back. However, the same experiment could be repeated in the O band where the interplay between dispersion and phase modulation is minimized

and reach could be extended. The last experiment in [20] for the 4D format was also performed in the C band, but dispersion pre-compensation using DSP was used at the transmitter prior to driving the DP-IQ modulator in the last line of Fig. 13.3. One final comment on Table 13.1, we should notice that the increase in bit rate from 300 to 320 Gb/s by going from 3D to 4D modulation format seems marginal; however, this increase was realized at a reduced symbol rate (40 instead of 50 Gsym/s) due to the more spectrally efficient 4D format. This means all the electronic, the electro-optic, and the optoelectronic components required can have smaller bandwidths since they will run at a slower signaling rate.

Finally, we should also note that the results in Table 13.1 were achieved using transceivers realized from discrete optical components (e.g., notice the fiber-based couplers, polarization controllers, and optical delay lines in Fig. 13.6). However, all these transceivers depicted in Fig. 13.3 can be potentially integrated on photonic ICs. Refs. [21–23] give examples from the literature of Stokes transmitters and receivers demonstrated experimentally as silicon photonic integrated circuits.

13.6 Conclusion and Future Research Avenues

In this chapter, we presented a review of multidimensional modulation formats which can be direct-detected without a local oscillator laser. These formats are capable of modulation up to four dimensions of a single laser being the intensity on orthogonal polarization states, the inter-polarization phase, and the inter-polarization differential phase. Due to their ability to deliver much larger bit rates at similar symbol rates compared to legacy one-dimensional formats such as OOK, these multidimensional formats are candidates to be deployed in next-generation intra-DC optical interconnects. Using these formats, the number of wavelengths or fiber lanes required to be multiplexed to achieve a target aggregate capacity can be greatly reduced by pushing the per-channel bit rate. The transceiver architectures are depicted together with the enabling digital signal processing required to invert the polarization rotation along the fiber and detect all dimensions carrying modulated data. Experimental results obtained using benchtop discrete components to realize the transceivers as well as offline DSP were also highlighted.

Moving forward, potential research avenues include exploring alternative implementations of multidimensional transceivers that are less complex than the ones already presented. In particular, improvements in receiver sensitivity are highly desirable which can be achieved by using different optical front-ends. Also, fully integrated transceivers should be realized which requires, in addition to PIC fabrication, extensive optical and electrical packaging endeavors. Finally, a more in-depth study of the power consumption of the transceivers including the DACs, ADCs, drivers, and real-time DSPs implemented as application-specific ICs (ASICs) should be performed. Such power consumption study will solidify the likelihood of implementing multidimensional formats in future optical interconnects over intra-DC reaches (<10 km).

References

1. Cisco Corporation, Cisco global cloud index: forecast and methodology, 2015–2020 (2016). Cisco white paper available at http://www.cisco.com/c/dam/en/us/solutions/collateral/ service-provider/global-cloud-index-gci/white-paper-c11–738085.pdf
2. E. Agrell, M. Karlsson, A. Chraplyvy, et al., Roadmap of optical communications. J. Opt. **18**, 063002 (2016)
3. B. Booth, in *Lighting up the cloud. presented at photonic integrated circuits (PIC) international conference*, Brussels, Belgium, 1–2 March 2016
4. IEEE, P802.3bs 200 Gb/s and 400 Gb/s Ethernet Task Force [Online]. Available at http://www.ieee802.org/3/bs/index.html
5. G. Agrawal, *Lightwave Technology Telecommunication Systems* (Wiley-Interscience, Hoboken, 2005)
6. M. Chagnon, M. Morsy-Osman, D. Patel, et al., Digital signal processing for dual-polarization intensity and inter-polarization phase modulation formats using stokes detection. J. Lightw. Technol. **34**, 188–195 (2016)
7. Y. Kai, M. Nishihara, T. Tanaka et al., Experimental comparison of pulse amplitude modulation (PAM) and discrete multi-tone (DMT) for short-reach 400-Gbps data communication. Paper presented at 39th European Conference on Optical Communication (ECOC), London, UK, 22–26 September 2013
8. A. Karar, J. Cartledge, Generation and detection of a 112-Gb/s dual-polarization signal using a directly modulated laser and half-cycle 16-QAM Nyquist-subcarrier-modulation. Paper presented at Post-deadline session of 38th European Conference on Optical Communication (ECOC), Amsterdam, Netherlands, 16–20 September 2012
9. M. Olmedo, T. Zuo, J. Jensen, et al., Multiband carrierless amplitude phase modulation for high capacity optical data links. J. Lightw. Technol. **32**, 798–804 (2014)
10. M. Chagnon, M. Morsy-Osman, M. Poulin, et al., Experimental study of 112 Gb/s short reach transmission employing PAM formats and SiP intensity modulator at 1.3 μm. Opt. Express **22**, 21018–21036 (2014)
11. P. Winzer, R. Essiambre, Advanced optical modulation formats. Proc. IEEE **94**, 952–985 (2006)
12. M. Morsy-Osman, M. Chagnon, M. Poulin et al., 1λ × 224 Gb/s 10 km transmission of polarization division multiplexed PAM-4 signals using 1.3 μm SiP intensity modulator and a direct-detection MIMO-based receiver. Paper presented at Post-deadline session of 40th European Conference on Optical Communication (ECOC), Cannes, France, 21–25 September 2014
13. D. Che, A. Li, X. Chen et al., 160-Gb/s stokes vector direct detection for short reach optical communication. Paper presented at Post-deadline session of 37th Optical Fiber Communication (OFC) Conference, San Francisco, California, 9–14 March 2014
14. D. Che, A. Li, X. Chen, et al., Stokes vector direct detection for linear complex optical channels. J. Lightw. Technol. **33**, 678–684 (2015)
15. M. Sowailem, T. Hoang, M. Chagnon, et al., 100G and 200G single carrier transmission over 2880 and 320 km using an InP IQ modulator and stokes vector receiver. Opt. Express **24**, 30485–30493 (2016)
16. M. Chagnon, M. Osman, D. Patel et al., 1 λ, 6 bits/symbol, 280 and 350 Gb/s direct detection transceiver using intensity modulation, polarization multiplexing, and inter-polarization phase modulation. Paper presented at Post-deadline session of 38th Optical Fiber Communication (OFC) Conference, Los Angeles, California, 22–26 March 2015
17. M. Morsy-Osman, M. Chagnon, D. Plant, Polarization division multiplexed intensity, inter polarization phase and inter polarization differential phase modulation with stokes space direct detection for 1λ×320 Gb/s 10 km transmission at 8 bits/symbol. Paper presented at Post-deadline session of 41st European Conference on Optical Communication (ECOC), Valencia, Spain, 27 September – 1 October 2015

18. M. Chagnon, M. Morsy-Osman, M. Poulin, et al., Experimental parametric study of a silicon photonic modulator enabled 112-Gb/s PAM transmission system with a DAC and ADC. J. Lightw. Technol. **33**, 1380–1387 (2015)
19. M. Morsy-Osman, M. Chagnon, M. Poulin, et al., 224 Gb/s 10 km transmission of PDM PAM-4 at 1.3 μm using a single intensity-modulated laser and a direct-detection MIMO DSP-based receiver. J. Lightw. Technol. **33**, 1417–1424 (2015)
20. M. Morsy-Osman, M. Chagnon, D. Plant, Four dimensional modulation and stokes direct detection of polarization division multiplexed intensities, inter polarization phase and inter polarization differential phase. J. Lightw. Technol. **34**, 1585–1592 (2016)
21. P. Dong, X. Chen, K. Kwangwoong, et al., 128-Gb/s 100-km transmission with direct detection using silicon photonic Stokes vector receiver and I/Q modulator. Opt. Express **24**, 14208–14214 (2016)
22. P. Dong, X. Chen, Stokes vector communications using silicon photonic integrated circuits. Presented at OSA Asia Communications and Photonics Conference (ACP), Wuhan, China, 2–5 November 2016
23. E. Elfiky, M. Sowailem, A. Samani et al., Dual polarization O-Band silicon photonic intensity modulator for Stokes vector direct detection systems," to appear at 40th Optical Fiber Communication (OFC) Conference, Los Angeles, California, 19–23 March 2017